Biointerface Research in Applied Chemistry
Platinum Open Access Journal (ISSN: 2069-5837)

Article
Volume 11, Issue 1, 2021, 8538 - 8549
https://doi.org/10.33263/BRIAC111.85388549

Synthesis, FT-IR, Bandgap Offset, Polarizability and Hyperpolarizability of 3,4-diamino-6-ehtyl-6H-pyrano[3,2-c]quinoline-2,5-dione (DAPQ) and Cu-2DAPQ as a Promising Organometallic Material: Experimental and Theoretical Studies

Mohamed A.M. El-Mansy [1, 2], Mai A. Mostafa [3], Medhat A. Ibrahim [4,*]

[1] Molecular Modeling Simulation Lab., Department of Physics, Faculty of Education, Ain Shams University, Roxy, Cairo, Egypt
[2] Condensed Matter Theory Group, Department of Physics, College of Science and Arts, Qassim University, ArRass, 51921, Saudi Arabia
[3] Organic Chemistry Lab., Chemistry Department, Faculty of Education, Ain Shams University, Roxy, Cairo, Egypt
[4] Molecular Spectroscopy and Modeling Unit, Spectroscopy Department, National Research Centre, 33 El-Bohouth St., 12622 Dokki, Giza, Egypt
* Correspondence: medahmed6@yahoo.com;

Scopus Author ID 8641587100
Received: 2.07.2020; Revised: 29.07.2020; Accepted: 30.07.2020; Published: 2.08.2020

Abstract: In our research, a comparative experimental and computational IR spectra of DAPQ have performed utilizing B3LYP/6-311G level. DAPQ hold over total dipole moment (TDM) (5.18 Debye), and HOMO/LUMO offset (3.76 eV). A theoretical model has been established to inspect the interaction between Cu^{+4} and N atoms associated with $(-NH_2)_2$ terminals of DAPQ. TDM for Cu-2DAPQ has been improved by 70.38% (17.49 Debye). Also, Cu-2DAPQ spin became doublet, which gives rise to the band splitting into Alpha and Beta MOs with energies 2.58 and 1.31 eV, respectively. Moreover, Cu-2DAPQ hyperpolarizability (β_{tot}) is 200 times larger over urea (ref. β_{urea} = 0.3728 $x10^{-30}$ esu). Eventually, the non-linear optical response has been improved by 94.53%. Such outstanding improvement nominates Cu-2DAPQ as a promising MOF material for both Photovoltaic and non-linear optics applications.

Keywords: Organometallic; Density Functional Theory; Non-linear Optics; Polarizability and first Hyperpolarizability.

1. Introduction

A little while backward, researchers have paid more interest in metal/organic frameworks (MOFs) for fabricating newly efficient solar cells [1-3]. MOFs combine transition metal cations with multidentate organic materials. Such MOFs are applied in catalysis, sensing, and gas storage implementations. Moreover, MOFs can serve in various fields as nano/material science and drug-delivery techniques (DDTs) [4]. Organic solar cells are distinguished with fair cost manufacture and active competences for energy transmutation [4-6]. Researcher's prior challenge is to explore a high photo-current by a synthesis of new organic solar cells [7, 8]. Pyrano-quinoline-2-one derivatives are prominent by their bio-pharmaceutical significance as antitumor/antioxidant activities, protein control, and anti-bacterial/anti-fungal drug

synthesis leverages [9-11]. 3,4-diamino-6-ehtyl-6H-pyrano[3,2-c]quinoline-2,5-dione (DAPQ) is one of pyrano-quinoline-2-one derivatives which has a structural formulation as $C_{14}H_{13}N_3O_3$, and its molecular mass is 271.09569 amu as shown in Fig.1. In our research, a computer-based simulation program will be applied as a spectroscopic tool for DAPQ FT-IR spectrum authorization [12]. Theoretical iterations are based upon density functional theory (DFT) selecting Becke3–Lee–Yang–Parr (B3LYP) as precise means for computing Vibro-optical spectroscopy [13-15] as well as hetero-cyclic conjugations and optoelectronic features [16]. Molecular modeling at a different level of theories shows potential applications for elucidating molecular structures fro many systems and molecules [17-20]. Molecular modeling provides data not limited to physical, chemical, and biological properties but also could be of concern for conformers and isomers covering, organic, inorganic, and organometallic systems [21-24].

As further as informed, neither experimental nor theoretical insights have been reported for DAPQ molecule yet. In consequence, we represent the first announcement to study the experimental FT-IR spectrum of DAPQ. We select DFT/B3LYP/6-311G level to calculate various features as optimal geometry, IR, HOMO-LUMO band gaps, Total dipole moment (TDM), and thermo-chemistry. Non-linear optics (NLO), Polarizability and hyperpolarizability, has been calculated by WB97XD/6-311G level. Moreover, we investigate the interaction between terminal diamino groups $(-NH_2)_2$ of DAPQ with copper Cu^{+4} cations at the same level; to seek how the physical properties of Cu-2DAPQ will be improved for both photovoltaic and non-linear optics applications.

2. Materials and Methods

2.1. Synthesis of DAPQ.

The title compound was prepared for the first time by mixing 6-ethyl-3,4 dicholro-6H-pyrano[3,2-c]quinoline-2,5-dione (3.1 g, 10 mmol) with ammonium acetate (6.16 g, 80 mmol) for 3 h at 220 ºC under free-solvent circumstance [25]. The green powder precipitate so obtained was filtered off, washed by water (3 x10 mL), dried and crystallized from methanol to give DAPQ; Yield 1.70 g (62.7%); green crystals; mp 181-183 ºC; as shown in Fig.1.

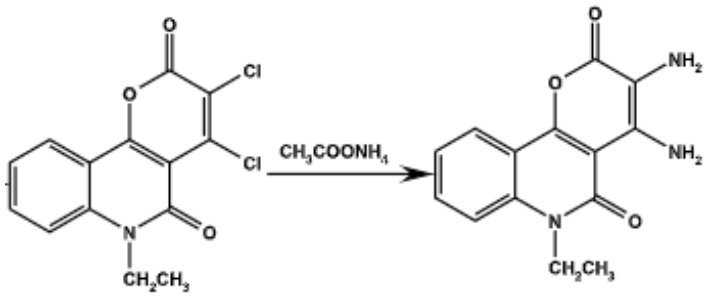

Figure 1. Synthesis scheme for DAPQ compound.

2.2. FT-IR spectrometry

A compressed DAPQ/KBr in a ratio (50:1) has been applied for the FT-IR spectrometer, which is adjusted to scan in the range 500–4000 cm^{-1} at chamber temperature.

2.3. Theory/Calculations.

Theoretical computations were fulfilled by DFT/B3LYP/6-311G level on PC Core I5/2.8 GHz through Gaussian (G09) [26] and GaussView 5 [27] programs. Initially, DAPQ geometrical optimization has been elaborated in Fig. 2(b). Subsequently, DAPQ IR frequencies have been calculated and compared with the observed one (see Fig.3). After that, thermo-physicochemical aspects, total dipole moment (TDM), HOMO/LUMO offset, nuclear repulsion energy, ionizing potential (I), electronic affinity (A), hardness (η), electronic potential (μ), electrophilic index (η) and lastly softness (ζ) have been calculated. In addition, DAPQ non-linear optical (NLO) features such as polarizability (α) and 1st order hyperpolarizability (β) have been computed by WB97XD/6-311G. In addition, we investigate the interaction between terminal diamino groups $(-NH_2)_2$ of DAPQ with copper Cu^{+4} cations at the same level to seek how the physical properties of Cu-2DAPQ will be improved for both photovoltaic and non-linear optics applications. Moreover, the density of state spectra (DOS) for both DAPQ and Cu-2DAPQ will be constructed through GaussSum 3 program.

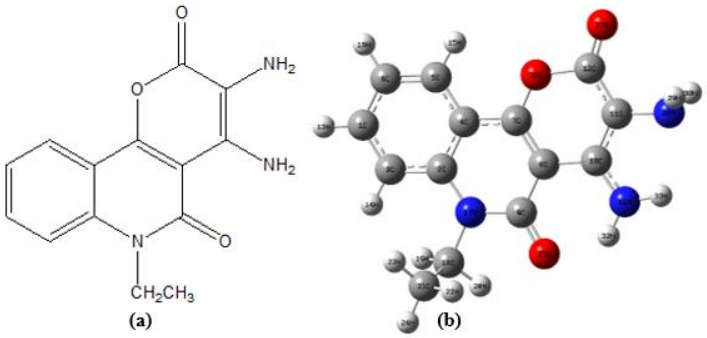

Figure 2. (a) Chemical construction; (b) Optimal geometry for DAPQ at B3LYP/6-311G.

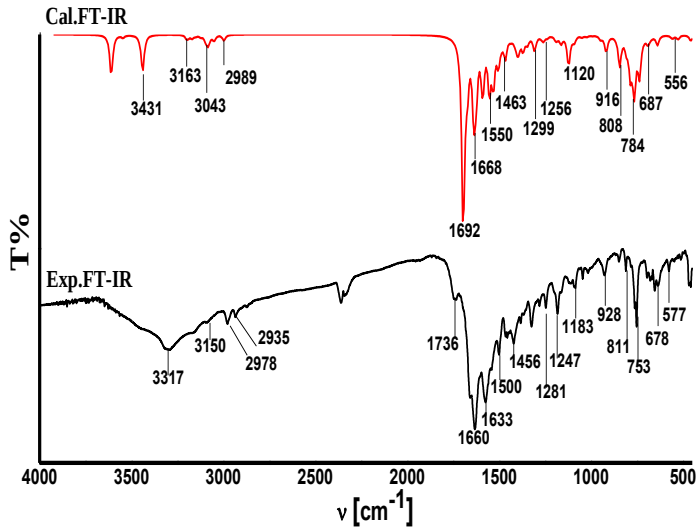

Figure 3. Observed and calculated FT-IR spectra for DAPQ at B3LYP/6-311G.

3. Results and Discussion

3.1. Optimum geometry.

The optimization process has revealed DAPQ crystal parameters (bond lengths & bond angles) at B3LYP/6-311G, which are imported into Table 1. Due to experimental data paucity on DAPQ crystallography, our reported results are considered as a reference map for discussion until others appear.

Table 1 Optimal bond lengths **(Å)** and bond angles **(°)** for DAPQ at B3LYP/6-311G.

Parameters					
Bond Length(Å)		Bond Angle (°)			
C1-C2	1.40	C2-C1-C6	121.08	O26-C12-O27	115.43
C1-C6	1.42	C2-C1-H13	119.10	C3-N17-C9	122.90
C1-H13	1.09	C6-C1-H13	119.83	C3-N17-C18	120.84
C2-C3	1.42	C1-C2-C3	120.32	C9-N17-C18	116.25
C2-H14	1.08	C1-C2-H14	118.94	N17-C18-H19	108.45
C3-C4	1.43	C3-C2-H14	120.74	N17-C18-H20	106.42
C3-N17	1.41	C2-C3-C4	118.48	C17-C18-C21	112.62
C4-C5	1.42	C2-C3-N17	121.89	H19-C18-H20	108.14
C4-C7	1.44	C4-C3-N17	119.63	H19-C18-C21	111.63
C5-C6	1.40	C3-C4-C5	120.36	H20-C18-C21	109.35
C5-H15	1.08	C3-C4-C7	118.22	C18-C21-H22	110.18
C6-H16	1.09	C5-C4-C7	121.42	C18-C21-H23	112.08
C7-C8	1.39	C4-C5-C6	120.48	C18-C21-H24	109.75
C7-O27	1.36	C4-C5-H15	118.09	H22-C21-H23	108.47
C8-C9	1.46	C6-C5-H15	121.42	H22-C21-H24	108.05
C8-C10	1.46	C1-C6-C5	119.28	H23-C21-H24	108.21
C9-N17	1.41	C1-C6-H16	120.29	C7-O26-C12	122.46
C9-O25	1.27	C5-C6-H16	120.43	C11-N28-H29	113.83
C10-C11	1.41	C4-C7-C8	121.80	C11-N28-H30	113.75
C10-N31	1.36	C4-C7-O26	115.87	H29-N28-H30	110.40
C11-C12	1.43	C8-C7-O26	122.33	C10-N31-H32	119.00
C11-N28	1.44	C7-C8-C9	119.88	C10-N31-H33	116.23
C12-O26	1.48	C7-C8-C10	118.35	H32-N31-H33	124.77
C12-O27	1.24	C9-C8-C10	121.78		
N17-C18	1.49	C8-C9-N17	117.53		
C18-H19	1.09	C8-C9-O25	122.93		
C18-H20	1.09	N17-C9-O25	119.53		
C18-C21	1.54	C8-C10-C11	119.57		
C21-H22	1.10	C8-C10-N31	120.83		
C21-H23	1.10	C11-C10-N31	119.60		
C21-H24	1.10	C10-C11-C12	122.58		
N28-H29	1.02	C10-C11-N28	117.86		
N28-H30	1.02	C12-C11-N28	119.56		
N31-H32	1.02	C11-C10-N31	114.72		
N31-H33	1.01	C11-C12-O27	129.85		

3.2. Vibrational assignments.

DAPQ ($C_{14}H_{13}N_3O_3$) as a non-linear structure possesses vibrational modes given by 3N-6, where N is the total atoms count. Accordingly, DAPQ dominates 93 (74 actives &19 inactive) modes. Only 17 modes opted to match with observed chart data assigned in Table 2. Proposed assignments are based upon GaussView 5 outputs for experimental/simulated IR wavenumbers. Computed wavenumbers have been factorized by 0.96 [28] to counterpart measurable peaks. Outstanding approval has been instituted between both measurable and calculated data. Fig. 3. show both DAPQ experimental and calculated IR spectra at B3LYP/6-311G. Outspread hydrogen antennas and griddle interactions may interfere agreement between measurable (solid-state) and predicted (gas state) data to some extent. Briefly, DAPQ assignments are discussed as in the following:

3.2.1. N-H, C-H vibrations.

N-H stretching detected near 3300 - 3500 cm^{-1} [29]. Mode (1) is assigned to N-H stretching at 3431 cm^{-1}, comparable to a measurable peak at 3317 cm^{-1}. Modes (9,14) are attributed to N-H in/out of plane bending at 1463 cm^{-1} and 808 cm^{-1}, corresponding to observed bands at 1456 cm^{-1} and 811 cm^{-1}, respectively.

C-H stretching (aromatic/aliphatic) perceived close to 3200–2900 cm^{-1} [30]. Modes (2,3,4) are specified to aromatic and asymmetric/symmetric C-H stretching at 3163, 3043, 2989 cm^{-1}, agreed with experimental data at 3150, 2978, 2935 cm^{-1}, respectively. Modes (10-12) are identified for C-H in-plane bending at 1299, 1256, 1120 cm^{-1}, proportionate to counted values at 1281, 1247, 1183 cm^{-1}. Mode (15) is related to C-H out of plane bending at 784 cm^{-1}, match with the recognized band at 753 cm^{-1}.

3.2.2. C=O, C=C vibrations.

C=O stretching is noticed around 1750-1690 cm^{-1} [31]. Mode (5) is specified for C=O stretching at 1692 cm^{-1}, proportionate to a recorded band at 1736 cm^{-1}. Modes (6-8) are referred to C=C stretching at 1668, 1634, 1550 cm^{-1}, balanced with experimental results at 1660, 1633, 1500 cm^{-1}.

3.2.3. C-O, C-N, C-C vibrations.

Mode (13) is related to C-O + C-N + C-C stretchings at 916 cm^{-1}, analogous to measured peak at 928 cm^{-1} [32]. Modes (16,17) are specified for C-O + C-N + C-C in/out of plane bendings at 687, 556 cm^{-1}, corresponding to recorded peaks at 678, 577 cm^{-1}, respectively.

Table 2 Experimental and calculated wavenumbers (cm^{-1}), IR intensities and assignments for DAPQ at B3LYP/6-311G.

No	Exp.	DAPQ				Species	Vibrational Assignments
		Wavenumber		IR intensity			
		Unscaled	Scaled	Rel.	Abs.		
1	3317	3501	3431	146	19	A’	υ N-H
2	3150	3228	3163	14	2	A'	υ C-H (aromatic)
3	2978	3106	3043	23	3	A'	υ_{as} C-H (aliphatic)
4	2935	3051	2989	24	3	A'	υ_{s} C-H (aliphatic)
5	1736	1727	1692	776	100	A'	υ C=O
6	1660	1703	1668	157	20	A'	υ C=C
7	1633	1668	1634	286	37	A'	
8	1500	1582	1550	208	27	A'	
9	1456	1493	1463	81	10	A'	β N-H
10	1281	1326	1299	7	1	A'	β C-H
11	1247	1282	1256	19	2	A'	
12	1183	1143	1120	121	16	A'	
13	928	935	916	66	9	A'	υ C-O + υ C-N + υ C-C
14	811	824	808	45	6	A"	γ N-H
15	753	801	784	146	19	A"	γ C-H
16	678	702	687	21	3	A'	β C-O + β C-N + β C-C
17	577	567	556	10	1	A"	γ C-O + γ C-N + γ C-C

υ (stretching); υ_{s} (Symmetric Stretching); υ_{as} (Asymmetric Stretching); β (in plane bending); γ (out of plane bending) Species; A' (stretching & in plane bending); A" (out of pane bending & deformations)

3.3. Mulliken distributions.

Mulliken distributions mark out electronegativity, charges carry, and the molecule's fine electronic arrays [33]. Detailed Mulliken charge distributions for DAPQ have been imported in Table 3 and plotted in Fig. 4. Our results showed that most acceptor atoms like O and N hold over negative charges due to their high electronegativity. Consequently, nearby carbon atoms C(3,4,7,8,9,10,12) exhibit positive charges, while others far away exhibit negative ones. Most hydrogens have positive charges due to their high donor property. Eventually, such electronegativity variance in DAPQ will impact both photovoltaic and non-linear optical features.

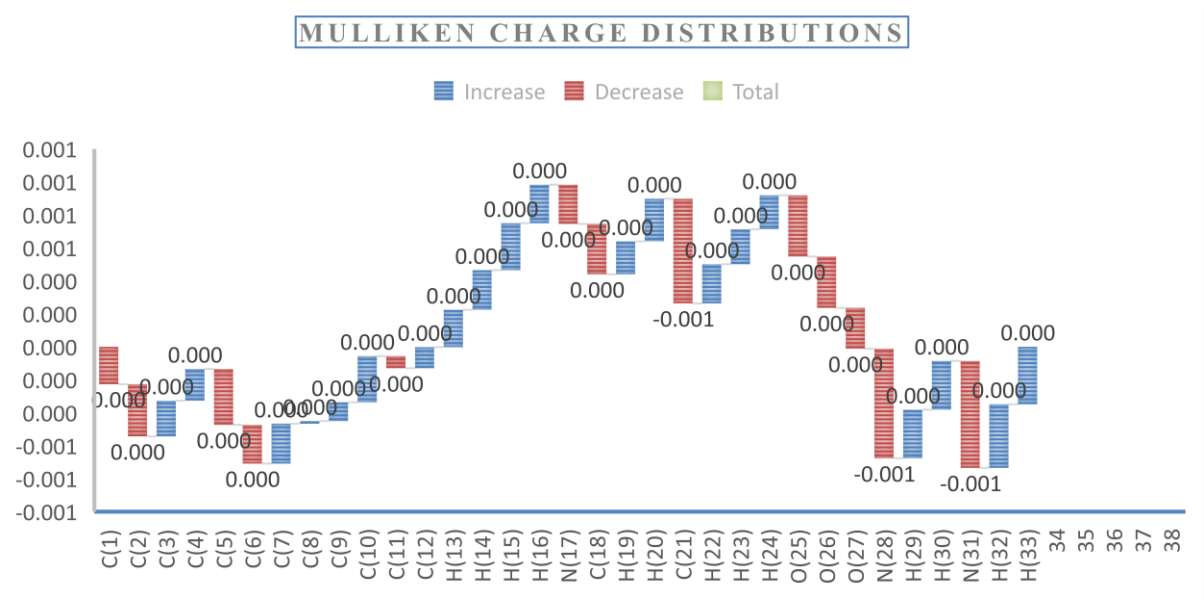

Figure 4. Mulliken charges transport distributions for DAPQ at B3LYP/6-311G.

Table 3. Mulliken charge distributions for DAPQ at B3LYP/6-311G.

Mulliken Charges Distributions (a.u)

Acceptors		Donors			
Atom		Atom		Atom	
C(1)	-0.226	C(3)	0.216	H(13)	0.226
C(2)	-0.316	C(4)	0.192	H(14)	0.240
C(5)	-0.340	C(7)	0.242	H(15)	0.285
C(6)	-0.234	C(8)	0.015	H(16)	0.233
C(11)	-0.074	C(9)	0.114	H(19)	0.200
C(18)	-0.305	C(10)	0.280	H(20)	0.258
C(21)	-0.634	C(12)	0.128	H(22)	0.237
				H(23)	0.212
O(25)	-0.372			H(29)	0.295
O(26)	-0.311			H(30)	0.296
O(27)	-0.248			H(32)	0.387
				H(33)	0.348
N(28)	-0.664				
N(31)	-0.649				
N(17)	-0.237				

3.4. Thermo-physicochemical features.

Conform to Koopman's postulate, through HOMO/LUMO energies essential physical parameters are specified like ionization potential I = -E_{HOMO}, electronic affinity A =-E_{LUMO}, hardness η =1/2(E_{LUMO}–E_{HOMO}), electronic potential μ= 1/2(E_{LUMO}+ E_{HOMO}), electrophilic index ψ = μ^2 /2η, and softness ζ = 1/η [34]. Spaciously, many assorted physical features have been listed (cf., Table 4) like total and zero-point energies, rotational constants, entropy S, specific heat C_V, total dipole moment (TDM), nuclear repulsion energy and HOMO-LUMO offset for DAPQ at the same level.

Table 4. Total & zero-point energies, rotational constants, entropies, molar specific heat C_V, total dipole moment, nuclear repulsion energy, E_{LUMO}, E_{HOMO}, HOMO-LUMO band gap, ionization potential, electron affinity, hardness, electronic potential, electrophilic index and softness for both DAPQ and Cu-2DAPQ.

Parameter	**DAPQ**	**Cu-2DAPQ**	
	B3LYP/6-311G	**B3LYP/6-311G**	
Total Energy (Hartree)	-931.1647326	-0.2088864	
Zero Point Energy (Kcal/Mol)	162.76354	302.8859	
Rotational Constants (GHz)	0.53269	0.12037	
	0.28194	0.04001	
	0.18803	0.03428	
Entropy (S) (Cal/Mol-°K)			
Total	130.181	245.804	
Transational	42.691	45.084	
Vibrational	33.698	38.807	
Rotational	53.793	160.536	
Molar Specific Heat (C_V) (Cal/Mol-°K)			
Total	65.961	144.71	
Transational	2.981	2.981	
Vibrational	2.981	2.981	
Rotational	59.999	138.749	
Nuclear repulsion energy (eV)	$4.163*10^4$	$6.988*10^4$	
Dipole Moment (Debye)	5.18	17.49	
Spin	Singlet	Doublet	
		Alpha MOs	Beta MOs
E_{LUMO} (eV)	-2.17	-2.93	-5.65
E_{HOMO} (eV)	-5.93	-5.52	-6.96
$E_{LUMO/HOMO}$ (eV)	3.76	2.58	1.31
Ionization energy (I) (eV)	2.17	2.93	5.65
Electron Affinity (A) (eV)	5.93	5.52	6.96
Global Hardness (η) (eV)	1.88	1.29	0.66
Chemical Potential (μ) (eV)	-4.05	-4.22	-6.31
Global Electrophilicity Index (ψ) (eV)	4.36	6.89	30.30
Softness (ζ) (eV^{-1})	0.53	0.77	1.52

3.5. Frontier bang gap energies.

HOMO/LUMO bandgap is a precise indicator of electron transit amongst molecular orbitals [35]. Fig. 5 (a-b) represents both predicted HOMO-LUMO energy gap and the electronic DOS spectrum for DAPQ. DAPQ holds over TDM (5.18 D), and HOMO/LUMO offset (3.76 eV). Most outstanding doorstep electron/hole pair generation energies for Si & Ge based solar are 3.9 eV and 2.8 eV, respectively [36]. In the upcoming period, DAPQ based solar cells will be the target for many researchers to check their efficiencies.

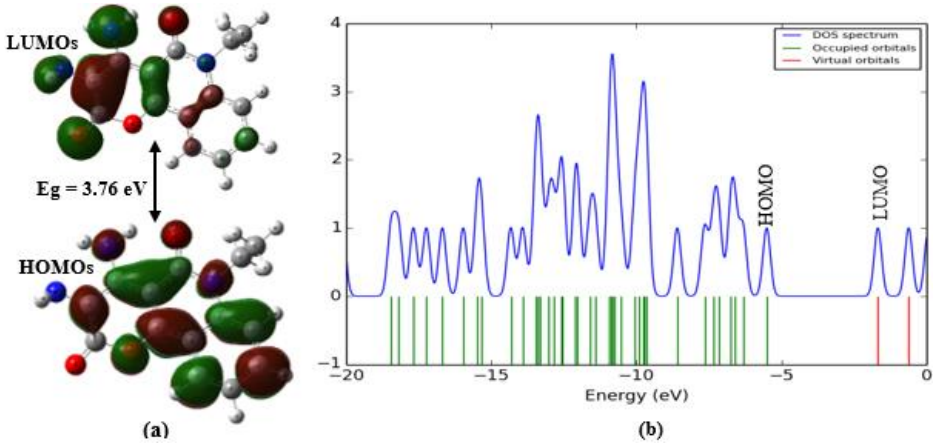

Figure 5. (a) HOMO/LUMO energy gap, (b) Electronic DOS spectrum for DAPQ at B3LYP/6-311G.

3.6. MOFs approach; Cu-2DAPQ construction and properties.

We theoretically inspect the interaction between Cu^{+4} and DAPQ dimer ($-NH_2$ groups). Cu-2DAPQ construction is based upon the interaction between Cu^{+4} cations with N atoms associated with $(-NH_2)_2$ terminals of DAPQ. Our results emphasize that Cu-2DAPQ dipole moment had been improved (17.49 Debye). Also, Cu-2DAPQ spin became doublet, which gives rise to the band splitting into Alpha and Beta MOs with energies 2.58 and 1.31 eV, respectively. Such surprising prediction would impact both spectral response and HOMO/LUMO offset by importing new transition probabilities for electron carry in original frontiers. Fig. 6 shows Cu-2DAPQ construction, calculated HOMO/LUMO band gaps, and DOS spectrum at the same level.

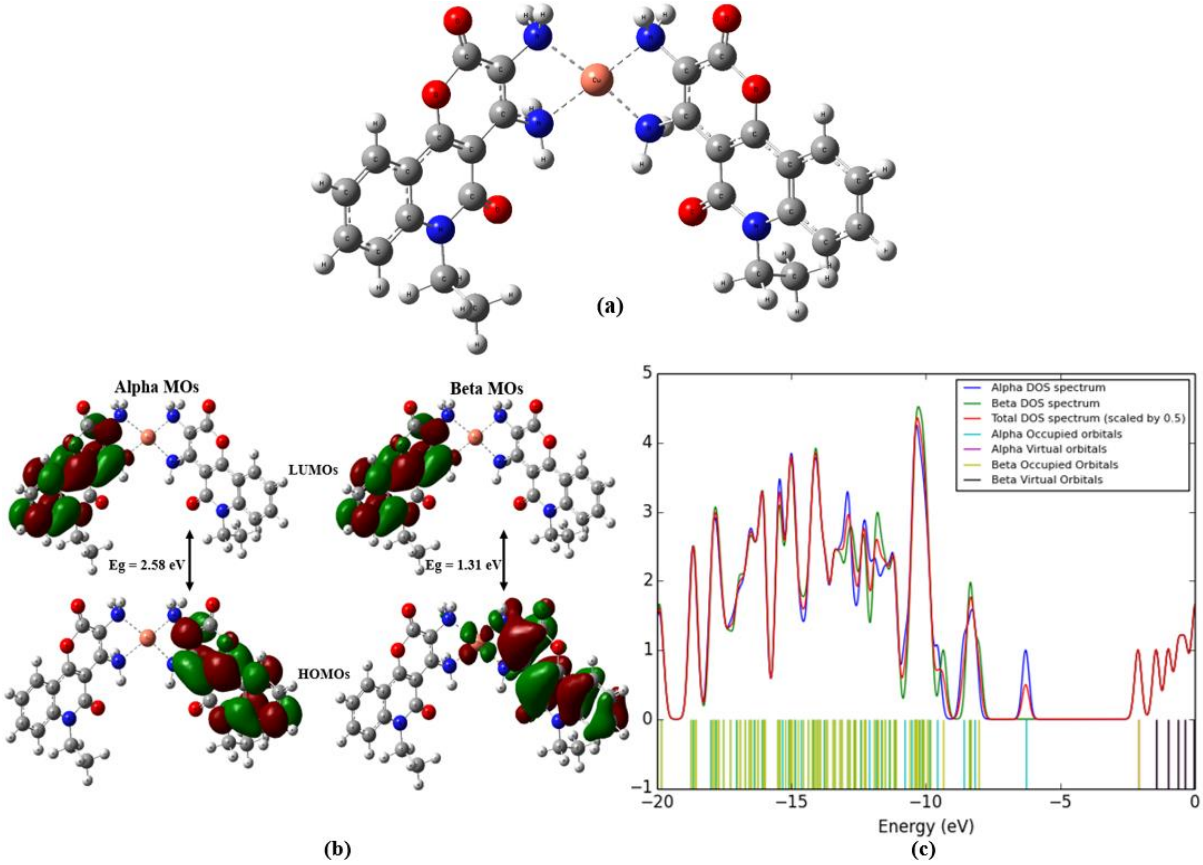

Figure 6. (a) construction; (b) HOMO/LUMO band gaps; (c) DOS spectrum for Cu-2DAPQ at B3LYP/6-311G.

3.7. Polarizability/first-order hyperpolarizability.

Hyperpolarizability and polarizability calculations have performed for both DAPQ and Cu-2DAPQ to investigate their non-linear optical (NLO) behaviors change upon copper coupling DAPQ dimer. Using gaussian output, we extract both polarizability (α_{xx}, α_{xy}, α_{yy}, α_{xz}, α_{yz}, α_{zz}) and hyperpolarizability (β_{xxx}, β_{xxy}, β_{xyy}, β_{yyy}, β_{xxz}, β_{xyz}, β_{yyz}, β_{xzz}, β_{yzz}, β_{zzz}) parameters. The total polarizability (α_{tot}), polarizability anisotropy ($\Delta\alpha$) and hyperpolarizability (β_{tot}) have been estimated using the subsequent empirical formulations [37]:

$$\alpha_{tot} = \frac{\alpha_{xx} + \alpha_{yy} + \alpha_{zz}}{3}$$

$$\Delta\alpha = \frac{1}{\sqrt{2}}\left[\left(\alpha_{xx} - \alpha_{yy}\right)^2 + \left(\alpha_{yy} - \alpha_{zz}\right)^2 + \left(\alpha_{zz} - \alpha_{xx}\right)^2 + 6\alpha_{yz}^2 + 6\alpha_{xy}^2 + 6\alpha_{xz}^2\right]^{1/2}$$

$$\beta_{tot} = \left[\left(\beta_{xxx} + \beta_{xyy} + \beta_{xzz}\right)^2 + \left(\beta_{yyy} + \beta_{yzz} + \beta_{yxx}\right)^2 + \left(\beta_{zzz} + \beta_{zxx} + \beta_{zyy}\right)^2\right]^{1/2}$$

Our predicted $\alpha_{tot}, \Delta\alpha$ *and* β_{tot} for both DAPQ and Cu-2DAPQ are listed in Table 5. A remarkable rise in $\alpha_{tot}, \Delta\alpha$ *and* β_{tot} of Cu-2DAPQ over prime DAPQ molecule. The calculated hyperpolarizability (β_{tot}) for both DAPQ and Cu-2DAPQ are 4.08 *x* 10^{-30} and 74.62 *x* 10^{-30} esu, respectively. The hyperpolarizability (β_{tot}) of Cu-2DAPQ is 200 times larger over urea (ref. β_{urea} = 0.3728 x10^{-30} esu). Eventually, the non-linear optical response has been improved by 94.53%. Such outstanding improvement nominates Cu-2DAPQ as promising MOF material for both Photovoltaic and non-linear optics applications.

Table 5. Mean polarizability α_{tot} (*x*10^{-24} esu), polarizability anisotropy $\Delta\alpha$ (*x*10^{-24} esu) and hyperpolarizability β_{tot} (*x*10^{-30} esu) for both DAPQ and Cu-2DAPQ at WB97XD/6-311G.

Parameters			**Parameters**		
	DAPQ	Cu-2DAPQ		DAPQ	Cu-2DAPQ
α_{xx}	35.62	62.25	β_{xxx}	1.47	-48.39
α_{xy}	-1.57	-8.48	β_{xxy}	1.63	26.28
α_{yy}	31.06	69.82	β_{xyy}	2.50	-11.80
α_{xz}	-0.56	-0.19	β_{yyy}	-3.05	8.40
α_{yz}	-0.85	4.84	β_{xxz}	-0.23	-0.36
α_{zz}	8.93	36.45	β_{xyz}	-0.20	4.37
α_{tot}	25.20	56.17	β_{yyz}	0.06	-8.98
$\Delta\alpha$	24.94	34.70	β_{xzz}	-0.12	-3.55
			β_{yzz}	0.07	3.49
			β_{zzz}	-0.01	2.34
			β_{tot}	4.08	74.62

(α; 1 a.u. = 0.1482×10^{-24} esu, β; 1 a.u. = 8.6393×10^{-33} esu)

Based on the presented computational data, one can conclude that molecular modeling data is of concern fro materials, whereas mechanism is required to fictionalize their behavior. The data given by molecular modeling is of great concern when the experimental data is limited and/or unavailable. These findings are in good agreement with the previous findings [38-40].

4. Conclusions

Our experimental and theoretical IR spectra of DAPQ have shown excellent approval for selected B3LYP/6-311G level accuracy. DAPQ holds over TDM (5.18 D), and HOMO/LUMO offset (3.76 eV). A theoretical model has been established to inspect the interaction between Cu^{+4} and N atoms associated with $(-NH_2)_2$ terminals of DAPQ. TDM for Cu-2DAPQ has been improved by 70.38% (17.49 Debye). Also, Cu-2DAPQ spin became

doublet, which gives rise to the band splitting into Alpha and Beta MOs with energies 2.58 and 1.31 eV, respectively. Moreover, Cu-2DAPQ hyperpolarizability (β_{tot}) is 200 times larger over urea (ref. β_{urea} = 0.3728 x10^{-30} esu). Eventually, the non-linear optical response has been improved by 94.53%. Such outstanding improvement nominates Cu-2DAPQ as a promising MOF material for both Photovoltaic and non-linear optics applications.

Funding

This research received no external funding.

Acknowledgments

This research has no acknowledgment.

Conflicts of Interest

The authors declare no conflict of interest.

References

1. Bortňák, D.; Milata, V.; Šofranko, J.; Végh, D.; Prousek, J.; Barbieriková, Z.; Breza, M.; Brezová, V.; Dvoranová, D.; Šoral, M. Unexpected Cleavage of N-N Bonds of Pentafluorophenylhydrazones – Formation of Nitriles by a Radical Fragmentation Reaction. *ChemistrySelect* **2020,** *5*, 3929-3933, https://doi.org/10.1002/slct.202001055.
2. El-Mansy, M.A.M. Quantum chemical studies on structural, vibrational, non-linear optical properties and chemical reactivity of indigo carmine dye. *Spectrochimica Acta Part A: Molecular and Biomolecular Spectroscopy* **2017,** *183*, 284-290, https://doi.org/10.1016/j.saa.2017.04.047.
3. Edgar, R.J.; Elliott, P.I.; Fennessy, R.V.; Gabbutt, C.D.; Heron, B.M.; Pope, S.J.; Sinopoli, A.; Rice, C.R. Inhibition of the photochromic behaviour of a 3,3-diphenyl-3*H*-pyrano[3,2-*f*]quinoline ligand by coordination to Ag(I) ions. *Dyes and Pigments* **2020,** *175*, https://doi.org/10.1016/j.dyepig.2019.108167.
4. Wang, Q.; Yang, Q.; Wu, W. Progress on Structured Biosensors for Monitoring Aflatoxin B1 From Biofilms: A Review. *Frontiers in Microbiology* **2020,** *11*, https://doi.org/10.3389/fmicb.2020.00408.
5. Baeyer, A.; Drewsen, V. *Darstellung von Indigblau aus Orthonitrobenzaldehyd. Berichte der deutschen chemischen Gesellschaft* **1882,** *15*, 2856-2864, https://doi.org/10.1002/cber.188201502274.
6. El-Mansy, M.A.M.; Yahia, I. Spectroscopic notes of Methyl Red (MR) dye. *Spectrochimica Acta Part A: Molecular and Biomolecular Spectroscopy* **2014,** *130*, 59-63, https://doi.org/10.1016/j.saa.2014.03.113.
7. El-Barbary, A.A.; El-Nahass, M.M.; Kamel, M.A.; El-Mansy, M.A.M. FT-IR, FT-Raman Spectra and Ab Initio HF, DFT Vibrational Analysis of P-methyl acetanilide. *Journal of Applied Sciences Research* **2009,** *11*, 1977-1987.
8. Brikci-Nigassa, N. M.; Nauton, L.; Moreau, P.; Mongin, O.; Duval, R. E.; Picot, L.; Thiéry, V.; Souab, M.; Baratte, B.; Ruchaud, S. Functionalization of 9-thioxanthone at the 1-position: From arylamino derivatives to [1]benzo(thio)pyrano[4,3,2-*de*]benzothieno[2,3-*b*]quinolines of biological interest. *Bioorganic Chemistry* **2020,** *94*, https://doi.org/10.1016/j.bioorg.2019.103347.
9. Soliman, H.; Yahia, I. Synthesis and technical analysis of 6-butyl-3-[(4-chlorophenyl)diazenyl]-4-hydroxy-2H-pyrano[3,2-c] quinoline-2,5(6H)-dione as a new organic semiconductor: Structural, optical and electronic properties. *Dyes and Pigments* **2020,** *176*, https://doi.org/10.1016/j.dyepig.2020.108199.
10. El-Mansy, M.A.M.; El-Nahass, M.; Khusayfan, N.; El-Menyawy, E. DFT approach for FT-IR spectra and HOMO–LUMO energy gap for *N*-(*p*-dimethylaminobenzylidene)-*p*-nitroaniline (DBN). *Spectrochimica Acta Part A: Molecular and Biomolecular Spectroscopy* **2013,** *111*, 217-222, https://doi.org/10.1016/j.saa.2013.04.018.
11. El-Mansy, M.A.M.; Ismail, M. On the spectroscopic analyses of 3-(4-Hydroxy-1-methyl-2-oxo-1,2-dihydro-quinolin-3-yl)-2-nitro-3-oxo-propionic acid (HMQNP). *Spectrochimica Acta Part A: Molecular and Biomolecular Spectroscopy* **2015,** *135*, 704-709, https://doi.org/10.1016/j.saa.2014.07.033.
12. El-Mansy, M.A.M.; Yahia, I. Spectroscopic notes of Methyl Red (MR) dye. *Spectrochimica Acta Part A: Molecular and Biomolecular Spectroscopy* **2014,** *130*, 59-63, https://doi.org/10.1016/j.saa.2014.03.113.
13. El-Nahass, M.; Kamel, M.; El-Barbary, A.; El-Mansy, M.A.M.; Ibrahim, M. FT-IR spectroscopic analyses of 3-Methyl-5-Pyrazolone (MP). *Spectrochimica Acta Part A: Molecular and Biomolecular Spectroscopy* **2013,** *111*, 37-41, https://doi.org/10.1016/j.saa.2013.03.072.

14. Ibrahim, M.A.; Badran, A. Synthesis and chemical reactivity of novelpyrano[3,2-c]quinoline-3-carbonitriles. *Synthetic Communications* **2020,** *50,* 1871-1882, https://doi.org/10.1080/00397911.2020.1759095.
15. Frisch, M.J.; Trucks, G.W.; Schlegel, H.B.; Scuseria, G.E.; Robb, M.A.; Cheeseman, J.R.; Montgomery, J.J.A.; Vreven, T.; Kudin, K.N.; Burant, J.C.; Millam, J.M.; Iyengar, S.S.; Tomasi, J.; Barone, V.; Mennucci, B.; Cossi, M.; Scalmani, G.; Rega, N.; Petersson, G.A.; Nakatsuji, H.; Hada, M.; Ehara, M.; Toyota, K.; Fukuda, R.; Hasegawa, J.; Ishida, M.; Nakajima, T.; Honda, Y.; Kitao, O.; Nakai, H.; Klene, M.; Li, X.; Knox, J.E.; Hratchian, H.P.; Cross, J.B.; Adamo, C.; Jaramillo, J.; Gomperts, R.; Stratmann, R.E.; Yazyev, O.; Austin, A.J.; Cammi, R.; Pomelli, C.; Ochterski, J.W.; Ayala, P.Y.; Morokuma, K.; Voth, G.A.; Salvador, P.; Dannenberg, J.J.; Zakrzewski, V.G.; Dapprich, S.; Daniels, A.D.; Strain, M.C.; Farkas, O.; Malick, D.K.; Rabuck, A.D.; Raghavachari, K.; Foresman, J.B.; Ortiz, J.V.; Cui, Q.; Baboul, A.G.; Clifford, S.; Cioslowski, J.; Stefanov, B.B.; Liu, G.; Liashenko, A.; Piskorz, P.; Komaromi, I.; Martin, R.L.; Fox, D.K.; Keith, T.; Al-Laham, M.A.; Peng, C.Y.; Nanayakkara, A.; Challacombe, M.; Gill, P.M.W.; Johnson, B.; Chen, W.; Wong, M.W.; Gonzalez, C.; Pople, J.A. Inc., Wallingford CT **2009**.
16. Frisch, A.; Dennington, R.; Keith, T.; Millam, J.; Nielsen, A.; Holder, A.; Hiscocks, J. Gaussian Inc., Wallingford, CT, USA **2009**.
17. Nazem, H.; Ghotbi, C.; Zare, M. H.; Shirazian, S. Experimental investigation and thermodynamic modeling of amino acids partitioning in a water/ionic liquid system. *Journal of Molecular Structure* **2018,** *260,* 386-390, https://doi.org/10.1016/j.molliq.2018.03.108.
18. Kawagoe, Y.; Surblys, D.; Matsubara, H.; Kikugawa, G.; Ohara, T. Construction of polydisperse polymer model and investigation of heat conduction: A molecular dynamics study of linear and branched polyethylenimine. *Polymers* **2019,** *180*, https://doi.org/10.1016/j.polymer.2019.121721.
19. Vergoten, G.; Bailly, C. N-glycosylation of High Mobility Group Box 1 protein (HMGB1) modulates the interaction with glycyrrhizin: A molecular modeling study. *Computational Biology and Chemistry* **2020**, https://doi.org/10.1016/j.compbiolchem.2020.107312.
20. Kushwaha, A.; Gupta, N.; Srivastava, J.; Singh, A.K.; Singh, M. Development of highly sensitive and selective sensor for ethionamide guided by molecular modelling *via* electropolymerized molecularly imprinted films. *Microchemical Journal* **2020,** *152*, https://doi.org/10.1016/j.microc.2019.104355.
21. Kobryn, A.E.; Gusarov, S.; Shankar, K. Multiscale modeling of active layer of hybrid organic-inorganic solar cells for photovoltaic applications by means of density functional theory and integral equation theory of molecular liquids. *Journal of Molecular Liquids* **2019,** *289*, https://doi.org/10.1016/j.molliq.2019.110997.
22. Kobryn, A. E.; Gusarov, S.; Shankar, K. Molecular simulations of oil adsorption and transport behavior in inorganic shale. *Journal of Molecular Liquids* **2019,** *305*, https://doi.org/10.1016/j.molliq.2020.112745.
23. Abdel-Karim, A.; Elhaes, H.; El-Kalliny, A.S.; Badawy, M.I.; Ibrahim, M.; Gad-Allah, T.A. Probing protein rejection behavior of blended PES-based flat-sheet ultrafiltration membranes: A density functional theory (DFT) study. *Spectrochimica Acta Part A: Molecular and Biomolecular Spectroscopy* **2020**, https://doi.org/10.1016/j.saa.2020.118399.
24. Refaat, A.; Elhaes, H.; Ammar, N.; Ibrahim, H.; Ibrahim, M. Green Route for the Removal of Pb From Aquatic Environment. *Combinatorial Chemistry & High Throughput Screening* **2020**, *23*, https://doi.org/10.2174/1386207323666200127123349.
25. Ibrahim, M.; El-Nahass, M.; Kamel, M.; El-Barbary, A.; Wagner, B.; El-Mansy, M.A.M. On the spectroscopic analyses of thioindigo dye. *Spectrochimica Acta Part A: Molecular and Biomolecular Spectroscopy* **2013,** *113*, 332-336, https://doi.org/10.1016/j.saa.2013.05.014.
26. Ismail, M.; Morsy, G.; Mohamed, H.; El-Mansy, M.A.M.; Abd-Alrazk, M. FT-IR spectroscopic analyses of 4-hydroxy-1-methyl-3-[2-nitro-2-oxoacetyl-2(1H)quinolinone (HMNOQ). *Spectrochimica Acta Part A: Molecular and Biomolecular Spectroscopy* **2013,** *113,* 191-195, https://doi.org/10.1016/j.saa.2013.04.117.
27. Soliman, H.; Eid, K. M.; Ali, H.; Atef, S.; El-Mansy, M.A.M. Vibrational spectroscopic analysis of 2-chloro-5-(2,5-dimethoxy-benzylidene)-1,3-diethyl-dihydro-pyrimidine-4,6(1H,5H)-dione. *Spectrochimica Acta Part A: Molecular and Biomolecular Spectroscopy* **2012,** *97,* 1079-1084, https://doi.org/10.1016/j.saa.2012.07.104.
28. Soliman, H.; Eid, K. M.; Ali, H.; El-Mansy, M.A.M.; Atef, S. FT-IR spectroscopic analyses of 2-(2-furanylmethylene) propanedinitrile. *Spectrochimica Acta Part A: Molecular and Biomolecular Spectroscopy* **2013,** *105,* 545-549, https://doi.org/10.1016/j.saa.2012.12.051.
29. Aly, A.A.; Ishak, E.A.; Shwaky, A.M.; Mohamed, A.H. Formation of furo[3,2-c]quinolone-2-carbonitriles and 4-oxo-4,5-dihydrofuro[3,2-c]quinolone-2-carboxamides from reaction of quinoline-2,4-diones with 2-[bis(methylthio)methylene]malononitrile. *Monatshefte für Chemie - Chemical Monthly* **2020,** *151*, 223-229, https://doi.org/10.1007/s00706-019-02541-0.
30. El-Mansy, M.A.M.; El-Nahass, M. On the spectroscopic analyses of Perylene-66. *Spectrochimica Acta Part A: Molecular and Biomolecular Spectroscopy* **2014,** *130,* 568-573, https://doi.org/10.1016/j.saa.2014.03.118.
31. Xiao, F.; Yao, S.; Wang, J.; Wei, J.; Amirkhanian, S. Physical and chemical properties of plasma treated crumb rubbers and high temperature characteristics of their rubberised asphalt binders. *Road Materials and Pavement Design* **2020,** *21*, 587-606, https://doi.org/10.1080/14680629.2018.1507922.

32. Chaudhary, J.P.; Kholiya, F.; Vadodariya, N.; Budheliya, V.M.; Gogda, A.; Meena, R. Carboxymethylagarose-based multifunctional hydrogel with super stretchable, self-healable having film and fiber forming properties. *Arabian Journal of Chemistry* **2020,** *13*, 1661-1668, https://doi.org/10.1016/j.arabjc.2017.12.034.
33. Edgar, R.J.; Elliott, P.I.; Fennessy, R.V.; Gabbutt, C.D.; Heron, B.M.; Pope, S.J.; Sinopoli, A.; Rice, C.R. Inhibition of the photochromic behaviour of a 3,3-diphenyl-3*H*-pyrano[3,2-*f*]quinoline ligand by coordination to Ag(I) ions. Dyes and Pigments. **2020,** *175*, https://doi.org/10.1016/j.dyepig.2019.108167.
34. Sureshkumar, B.; Mary, Y.S.; Panicker, C.Y.; Suma, S.; Armaković, S.; Armaković, S.J.; Van Alsenoy, C.; Narayana, B. Quinoline derivatives as possible lead compounds for anti-malarial drugs: Spectroscopic, DFT and MD study. *Arabian Journal of Chemistry* **2020,** 13, 632-648, https://doi.org/10.1016/j.arabjc.2017.07.006.
35. Aly, A.A.; Sayed, S.M.; Abdelhafez, E.S.M.; Abdelhafez, S.M.N.; Abdelzaher, W.Y.; Raslan, M.A.; Ahmed, A.E.; Thabet, K.; El-Reedy, A.A.; Brown, A.B. New quinoline-2-one/pyrazole derivatives; design, synthesis, molecular docking, anti-apoptotic evaluation, and caspase-3 inhibition assay. *Bioorganic Chemistry* **2020,** *94*, https://doi.org/10.1016/j.bioorg.2019.103348.
36. Gulácsi, M.; El-Mansy, M.A.M.; Gulácsi, Z. Electron-phonon interactions in conducting polymers. *Philosophical Magazine Letters* **2016,** *96*, 67-75, https://doi.org/10.1080/09500839.2016.1150611.
37. Chen, H.; Liu, M.; Yan, T. Molecular multipoles and (hyper)polarizabilities of water by *ab initio* calculations. *Chemical Physics Letters* **2020**, *752*, https://doi.org/10.1016/j.cplett.2020.137555.
38. El-Mansy, M.A.M.; Osman, O.; Mahmoud, A. A.; Elhaes, H.; Ibrahim, M. Computational notes on the molecular modeling analyses of flutamide. *Letters in Applied NanoBioScience* **2020**, *9*, 1099-1102, https://doi.org/10.33263/LIANBS92.10991102.
39. Ibrahim, A.; Elhaes, H.; Ibrahim, M. Computational notes on the electronic properties of carboxylic acid. *Letters in Applied NanoBioScience* **2020**, 9, 1079-1082, https://doi.org/10.33263/LIANBS92.10791082.
40. El-Mansy, M.A.M.; Osman, O.; Mahmoud, A.A.; Elhaes, H.; Gawad, A.E.D.A.; Ibrahim, M. Computational Notes on the Chemical Stability of Flutamide. *Letters in Applied NanoBioScience* **2020,** *9*, 1147–1155.